Supercond. Sci. Technol. **9** (1996) 1–15. Printed in the UK

TOPICAL REVIEW

High-frequency vortex dynamics in $YBa_2Cu_3O_7$

M Golosovsky, M Tsindlekht and D Davidov

Hebrew University of Jerusalem, Racah Institute of Physics, Jerusalem 91904, Israel

Received 25 September 1995

Abstract. We present a phenomenological description of the high-frequency vortex dynamics in $YBa_2Cu_3O_7$ and discuss the main parameters related to vortex motion, namely the viscous drag coefficient η, the pinning constant k_p (Labusch parameter) and the depinning frequency ω_0. We demonstrate experimental results on the angular and temperature dependence of η, k_p and ω_0 in $YBa_2Cu_3O_7$ and compare these results with existing models. We show how studies of the vortex viscosity may yield information on the superclean limit. This limit corresponds to the formation of the discrete excitation spectrum in the vortex core due to quantum confinement and small coherence length. From the low-temperature viscosity data we conclude that the superclean limit in $YBa_2Cu_3O_7$ is reached for magnetic field perpendicular to the *c*-axis.

1. Introduction

Vortex dynamics has attracted renewed attention with the advent of high-T_c superconductors [1, 2]. Recently, many new fascinating phenomena related to vortices in superconductors have been discovered: the irreversibility line, the vortex phase transition [1, 3] etc. There is a substantial theoretical effort to account for these effects. The theories of vortex motion [1, 2] operate with microscopic parameters of vortices, such as viscosity, pinning potential, pinning constant and Hall constant. Therefore, the experimental determination of these parameters is very important. High-frequency methods are particularly suitable for this purpose because they probe vortex response at very low currents when the vortices undergo *reversible* oscillations and they are less sensitive to the flux creep. The aim of this work is to review experimental data on the vortex viscosity, pinning constant and depinning frequency in high-T_c superconductors with the main emphasis on $YBa_2Cu_3O_7$.

Vortices in type-II superconductors may be considered as tubes with a normal core of radius ξ carrying a quantum of magnetic flux Φ_0 [4] (see figure 1). Many $YBa_2Cu_3O_7$ samples are in a clean limit, i.e. $\xi \ll l$, where l is the mean free path. This results in the negligible scattering of quasiparticles in the vortex core (for the motion perpendicular to the vortex axis). Due to very small lateral size of the vortex core, there is an analogy between a vortex in clean superconductors and mesoscopic systems [5] such as quantum wires. One expects that several phenomena, known for mesoscopic systems, such as level quantization and localization (arising from disorder along a vortex line) may occur in the vortex core. For example, it was predicted long ago that the quasiparticle excitation spectrum in the vortex core may be quantized [6]. This corresponds to the so-called superclean limit [7]. There are good reasons to believe that it may be realized in $YBa_2Cu_3O_7$ [8, 9] and $Bi_2Sr_2CaCu_2O_8$ [10]. We will show how studies of the vortex viscosity may yield information about this superclean limit.

2. Forces acting on vortices

2.1. Lorentz (Magnus) force

An electric current exerts a Lorentz force on the vortex. For a vortex at rest, this force can be expressed as $\boldsymbol{F}_L = \rho_s\Phi_0[\boldsymbol{v}_s \times \boldsymbol{n}]$ (or $\Phi_0[\boldsymbol{J} \times \boldsymbol{n}]$), where $\boldsymbol{n}$ is the unit vector directed along the vortex, ρ_s is the charge density of the condensate, $\boldsymbol{v}_s$ is the velocity of the condensate and $\boldsymbol{J}$ is the current density. This force drives the vortex perpendicular to the current. However, a vortex, moving with velocity $\boldsymbol{v}$, experiences an additional force $\rho_s\Phi_0[\boldsymbol{v} \times \boldsymbol{n}]$ that drives it along the current. Consequently, the Lorentz force on the moving vortex is modified to be $\boldsymbol{F} = \rho_s\Phi_0[(\boldsymbol{v}_s - \boldsymbol{v}) \times \boldsymbol{n}]$ [1, 10–13]. We emphasize that the Magnus force $\rho_s\Phi_0[\boldsymbol{v} \times \boldsymbol{n}]$ is responsible for the Hall effect. The Hall coefficient in this simple model is $\alpha_H = \rho_s\Phi_0$. (For a more rigorous derivation of the Hall coefficient see Ao and Thouless [12] and Feigelman *et al* [13].)

2.2. Viscous force

A vortex has a normal-state core. When a vortex moves, the quasiparticles in the core do not move with it (figure 1). Instead, the Cooper pairs on the front side of the core

0953-2048/96/010001+15$19.50

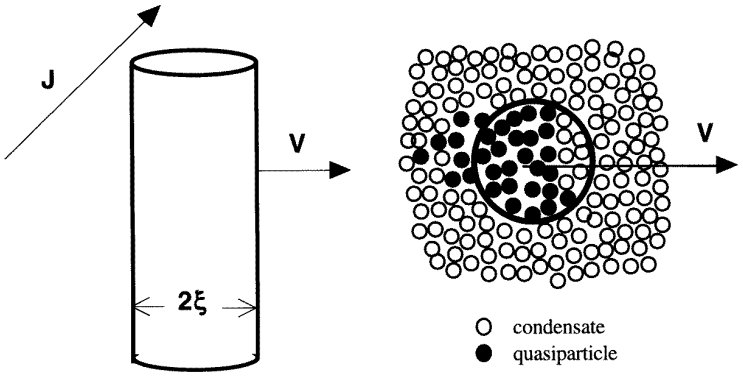

Figure 1. A vortex moves under the action of the transport current $\boldsymbol{J}$. The right-hand side shows a cross section of the moving vortex. On the front of the moving vortex the condensate is converted to quasiparticles, while on the rear of the vortex the quasiparticles are converted back to condensate.

are converted to quasiparticles through Andreev reflection [14] and energy is lost. On the rear side of the vortex core, the quasiparticles are converted back to Cooper pairs and some energy is restored. However, due to finite relaxation time, not all the energy is restored so the moving vortex dissipates. In other words, there is a viscous force $\boldsymbol{F}_{\rm v} = \eta \boldsymbol{v}$, where η is the viscous drag coefficient. This is Tinkham's mechanism of vortex dissipation [4]. There is also the Bardeen–Stephen mechanism arising from the Joule dissipation inside the normal-state core [15–17]. Both mechanisms yield similar expressions for the viscosity coefficient [4] (the difference appears [17] only in the close vicinity of $T_{\rm c}$). The total viscosity is [4]

$$\eta \approx \frac{\mu_0 H_{\rm c2} \Phi_0}{\rho_{\rm n}}. \tag{1}$$

Here $H_{\rm c2}$ is the critical field and $\rho_{\rm n}$ is the normal-state resistivity. Using the expression $\rho_{\rm n} = m^*/ne^2\tau$ and equation (1), we find

$$\eta = \pi \hbar n \omega_{\rm c} \tau. \tag{2}$$

Here n and τ are the quasiparticle concentration and relaxation time in the vortex core, and $\omega_{\rm c} = e\mu_0 H_{\rm c2}/m^*$ is the cyclotron frequency in the field $H_{\rm c2}$. The Bardeen–Stephen [15] derivation of viscosity is based on the hydrodynamic approach. This approach is valid in the limit $\omega_{\rm c}\tau \ll 1$, when there is a continuum spectrum of the excitations in the vortex core. Blatter *et al* [1] calculated vortex viscosity η and Hall constant $\alpha_{\rm H}$ for arbitrary values of $\omega_{\rm c}\tau$ and found

$$\eta = \pi \hbar n \frac{\omega_{\rm c}\tau}{1 + (\omega_{\rm c}\tau)^2} \tag{3a}$$

$$\alpha_{\rm H} = \pi \hbar n \frac{(\omega_{\rm c}\tau)^2}{1 + (\omega_{\rm c}\tau)^2} \tag{3b}$$

$$\tan \Theta_{\rm H} = \frac{\alpha_{\rm H}}{\eta} = \omega_{\rm c}\tau. \tag{3c}$$

Here $\Theta_{\rm H}$ is the Hall angle. Equations (3*a*) and (3*b*) show that in the limit $\omega_{\rm c}\tau \ll 1$ the viscosity is given by the Bardeen–Stephen expression ($\eta \approx \pi \hbar n \omega_{\rm c}\tau$) and the Hall effect is negligible ($\alpha_{\rm H} \ll \eta$). In the opposite limit, $\omega_{\rm c}\tau \gg 1$, the Hall effect is dominant ($\alpha_{\rm H} \approx \pi \hbar n \gg \eta$) and the viscosity can be expressed as $\eta \approx \pi \hbar n/\omega_{\rm c}\tau$. This corresponds to the superclean limit [6–9]. In this limit there are well-separated bound states in the vortex core (see figure 2).

The origin of these bound states is the quantum confinement of quasiparticles inside vortex core with diameter $\delta x \approx 2\xi$. The energy separation between bound states may be estimated as follows: the momentum is found from the uncertainty principle as $\delta p \approx \pi \hbar/\xi$. Using the BCS expression for the coherence length $\xi = \hbar v_{\rm F}/\pi\Delta$, where Δ is the gap energy and $v_{\rm F}$ is the Fermi velocity, one finds a level separation $\Delta E \approx \pi^4 \Delta^2/4E_{\rm F}$. Here $E_{\rm F}$ is the Fermi energy. A rigorous calculation [1, 6, 7] yields a level separation

$$\Delta E = \frac{\Delta^2}{E_{\rm F}} = \hbar \omega_{\rm c}. \tag{4}$$

The width of these levels is also estimated from the uncertainty principle as $\delta E \approx \hbar/\tau$. Therefore, the ratio of the level spacing ΔE to the level width δE is directly related to the parameter $\omega_{\rm c}\tau$:

$$\frac{\Delta E}{\delta E} = \omega_{\rm c}\tau. \tag{5}$$

The level quantization introduces a new energy scale $\Delta^2/E_{\rm F}$ which should be compared to kT. Therefore there are two regimes in the superclean limit: $\Delta^2/E_{\rm F} \ll kT$ and $\Delta^2/E_{\rm F} \gg kT$. In the low-temperature regime the viscosity is predicted to be dramatically different from that given by equation (3*a*) [18].

2.3. Pinning force

Vortices interact with various defects in the crystal lattice and are effectively pinned. The vortex motion in the presence of pinning sites may be described as a motion in some pinning potential. Under the action of a small alternating current, a vortex undergoes small oscillations in the potential well (figure 3(*a*)). There is a restoring

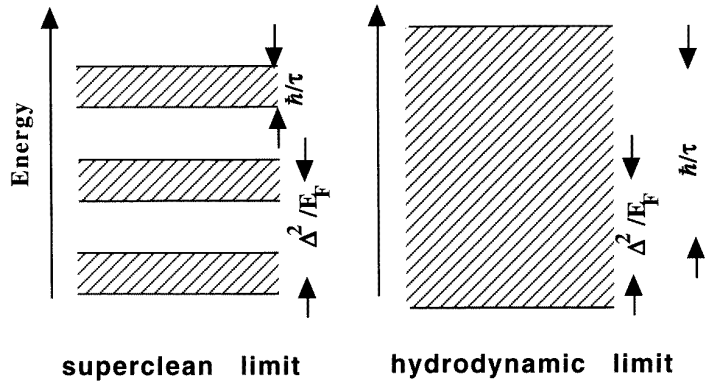

Figure 2. In the superclean limit there are well-separated bound states inside the vortex core. In the hydrodynamic limit these bound states are broadened and their overlap results in a continuum excitation spectrum.

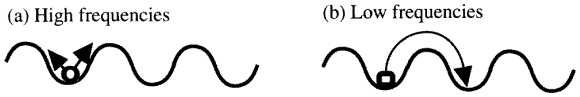

Figure 3. Vortex motion under the action of an alternating current J_{ac}. (*a*) At high frequencies the vortex is confined within a potential well $U(x)$. The vortex undergoes small oscillations and its motion is determined by the balance between pinning and viscous forces. (*b*) At lower frequencies hopping to an adjacent potential well (flux creep) may occur.

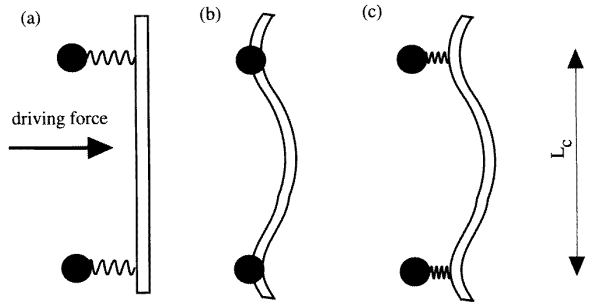

Figure 4. The pinning constant in several limiting cases. (*a*) Rigid vortex and weak pinning sites. The pinning constant is the spring coefficient of the restoring force exerted by the pinning sites. (*b*) Elastic vortex and very strong pinning sites. The pinning constant is determined by the line tension of the vortex and not by the properties of the pinning sites. (*c*) General case. The pinning constant is determined by the vortex elasticity and by the strength of the pinning sites as well. L_c is the average distance between pinning sites (correlation length along the vortex).

(pinning) force which is proportional to displacement: $\boldsymbol{F}_{\rm pin} = k_{\rm p}\boldsymbol{x}$. This force originates from the interaction with the pinning sites (figure 4(*a*)) and from the short-range vortex elasticity (figure 4(*b*)). The restoring force coefficient $k_{\rm p}$ is the pinning constant or Labusch parameter [19]. (Sometimes the pinning constant is defined differently, as the spring coefficient of the bulk pinning force [4], i.e. $k_p B/\Phi_0$. We will not use this definition.)

There are two main regimes of vortex pinning: individual pinning and collective pinning (figure 5). Individual pinning is realized at low fields, when there are few vortices and many pinning sites. In this regime the pinning constant does not depend on the vortex concentration (i.e. on magnetic field). Collective pinning is realized at higher fields when the vortex concentration is high and there are many vortices per pinning site. In this regime the pinning constant is smaller and field dependent (in conventional superconductors $k_{\rm p} \sim B^{-1/2}$ [20, 21]). (We point out that the notion 'collective pinning' has two different connotations. One of them (which we use throughout the present work) describes the situation when there are many vortices per pinning site. Another one (which we do not use) describes the pinning of a flexible vortex by a whole ensemble of pinning points. A flexible vortex deviates from the straight line in order to accommodate the pinning potential created by randomly distributed pinning points. In such a way the flexible vortex is pinned by the whole ensemble of pinning sites, which a rigid vortex can not accommodate and each pinning site acts it independently.) The pinning constant has a clear physical meaning for individual pinning (interaction of a single vortex with one or several pinning sites), while for collective pinning it is a result of statistical summation over many vortices and pinning sites. We will focus our attention on the individual pinning.

There are two major sources of the pinning: electromagnetic and core pinning [4]. Electromagnetic pinning [22] arises, for example, when the supercurrent pattern around the vortex is disturbed due to the presence of a non-conducting defect. Core pinning arises, for example, when a vortex core sticks to a normal-state inclusion. Since condensation energy is lost in the vortex core, some part of this energy is restored upon such sticking. A useful insight into the physical meaning of the pinning constant may be obtained from the following non-rigorous estimate [23, 24]. The core energy is spread over a distance 2ξ. Optimal core pinning is achieved by a defect of the same size. Assuming an infinite linear (or planar) defect and equating the linear core energy $\mu_0 H_{\rm c}^2 \xi^2/8$ (here $H_{\rm c}$ is the thermodynamic critical field) to the elastic energy $k_{\rm p}\xi^2/2$, the core pinning constant is estimated as

$$(k_{\rm p}^{\rm max})_{\rm core} \approx 0.25\mu_0 H_{\rm c}^2(t). \qquad (6)$$

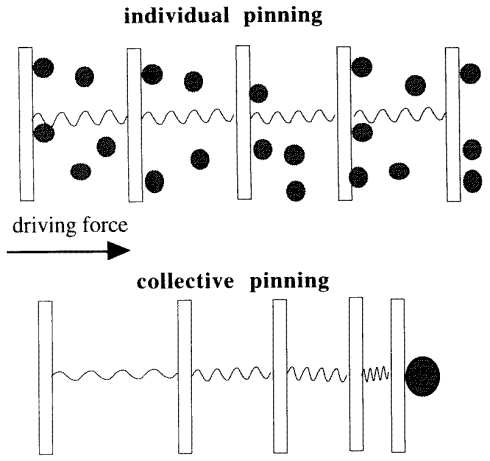

Figure 5. Individual versus collective pinning. Rods represent vortices, springs represent coupling between vortices, hatched circles represent pinning centres. In the individual pinning regime, there are many pinning sites per vortex and the pinning constant is field independent. In the collective pinning regime, there are many vortices per pinning site, the pinning constant is smaller and field dependent.

This simple estimate is modified when the vortex elasticity [1] is taken into account. Indeed, in the limiting case of rigid vortices (figure 4(*a*)), the pinning constant is the curvature of the pinning potential in the bottom of the potential well, i.e. $(k_\mathrm{p})_\mathrm{rigid} \approx L_\mathrm{c}^{-1}(\mathrm{d}^2U_\mathrm{c}/\mathrm{d}x^2)_{x=0}$. Here, L_c is the average distance between pinning sites (correlation length along the vortex). In the limiting case of flexible vortices and very strong pinning sites (figure 4(*b*)) the pinning constant may be estimated by analogy with elastic string as $(k_\mathrm{p})_\mathrm{elastic} \sim e_\mathrm{l}/L_\mathrm{c}^2$. Here e_l is the vortex line tension [1, 4]

$$e_\mathrm{l} = \frac{\mu_0 H_{\mathrm{c}1}\Phi_0}{4\pi\lambda^2}. \tag{7}$$

In the general case (figure 4(*c*)), the pinning constant is determined by vortex interaction with the pinning sites and by vortex elasticity as well. Blatter *et al* [1] estimate the pinning potential U_c and the correlation length L_c for the general case as follows:

$$U_\mathrm{c} = \mu_0 H_\mathrm{c}^2 \varepsilon \xi^3 \left(\frac{\delta}{\varepsilon}\right)^{1/3} \tag{8a}$$

$$L_\mathrm{c} = \varepsilon\xi \left(\frac{\delta}{\varepsilon}\right)^{-1/3}. \tag{8b}$$

Here ε is an anisotropy parameter and δ/ε is a dimensionless parameter which depends on the strength of the pinning potential. Assuming a very short-range potential (i.e. pinning radius $r_\mathrm{p} \approx \xi$), we estimate the upper limit on the pinning constant as $(k_\mathrm{p})^\mathrm{max} \approx U_\mathrm{c}/\xi^2 L_\mathrm{c} = \mu_0 H_\mathrm{c}^2(\delta/\varepsilon)^{2/3}$. For several strong pinning mechanisms in $YBa_2Cu_3O_7$ Blatter *et al* [1] obtain $\delta/\varepsilon \approx (10^{-2}\text{–}10^{-3})(1-t)^{-1/2}$ where $t = T/T_\mathrm{c}$ (in contrast to equation (6) this estimate includes both core and electromagnetic pinning). Since $H_\mathrm{c}(t) = H_\mathrm{c}(0)(1-t^2)^2$, equations (8*a*, *b*) yield

$$k_\mathrm{p} = (0.01 - 0.05)\mu_0 H_\mathrm{c}^2(0)(1-t)^{4/3}(1+t)^2. \tag{9}$$

This realistic estimate is several times smaller than a simple one given by equation (6).

3. Phenomenology of the vortex dynamics

The balance of forces determines the vortex equation of motion. The effect of thermal fluctuations is accounted for by a stochastic thermal force. The vortex motion is described by the Langevin-type equation [1, 25–27]

$$\eta\boldsymbol{v} + \alpha_\mathrm{H}[\boldsymbol{n}\times\boldsymbol{v}] + \partial U/\partial x = \Phi_0[\boldsymbol{n}\times\boldsymbol{J}] + \text{stochastic thermal force}. \tag{10}$$

Here $\boldsymbol{J}\mathrm{e}^{\mathrm{i}\omega t}$ is the transport current density, $\boldsymbol{x}$ and $\boldsymbol{v}$ are the vortex displacement and velocity, $\boldsymbol{n}$ is the unit vector along the vortex, η is the viscosity coefficient, α_H is the vortex Hall constant U is the pinning potential, and k_p is the pinning constant (Labusch parameter) defined as $k_\mathrm{p}x = \partial U/\partial x|x \to 0$. The vortex resistivity is $\rho_\mathrm{v} = B\Phi_0 v/J$. Equation (10) describes the motion of an individual vortex and is a mean-field approximation; therefore it is not valid close to the vortex phase transition, where interaction between vortices plays a dominant role. The region of the phase transition is better described by the scaling model (see Wu *et al* [28] and references therein).

We omit the inertial term in equation (10). The inertial effects might be relevant for quantum creep [1, 10] and for vortex dynamics in the far infrared [29–32]. Since the present work is focused on a lower frequency range (microwave and millimetre waves), the effects related to the vortex mass are ignored.

3.1. Vortex resistivity neglecting Hall effect and flux creep

In this limit equation (10) is reduced to that proposed first by Gittleman and Rosenblum [21], i.e. $\eta\boldsymbol{v} + k_\mathrm{p}\boldsymbol{x} = \boldsymbol{F}_\mathrm{L}$. The vortex resistivity is $\rho_\mathrm{v} = B\Phi_0 v/J$:

$$\rho_\mathrm{v} = \frac{B\Phi_0}{\eta}\frac{1}{1+\mathrm{i}\omega_0/\omega} \tag{11a}$$

$$\omega_0 = \frac{k_\mathrm{p}}{\eta}. \tag{11b}$$

Equation (11) indicates that pinning forces dominate at low frequencies, while frictional forces dominate at high frequencies. The depinning (crossover) frequency ω_0 delineates the low- and high-frequency regimes. According to equation (11*a*), at high frequencies ($\omega \gg \omega_0$) the vortex resistivity is real, $\rho_\mathrm{v} = B\Phi_0/\eta$, and the vortex motion is highly dissipative. At low frequencies ($\omega \ll \omega_0$) the vortex resistivity is imaginary, $\rho_\mathrm{v} = -\mathrm{i}\omega B\Phi_0/k_\mathrm{p}$, and the vortex motion is almost non-dissipative. The different regimes of the vortex resistivities are shown schematically in figure 6. At low fields, each vortex is pinned individually, thereby the pinning constant and the depinning frequency are field independent. At high fields, pinning is collective and weak (figure 5), and the depinning frequency is lower due to decrease of the pinning constant. At higher fields equations (10) and (11) are no longer valid due to the proximity of the vortex phase transition. In the region of the phase transition the frequency dependence of the vortex resistivity becomes more complicated and the depinning frequency loses its meaning [28].

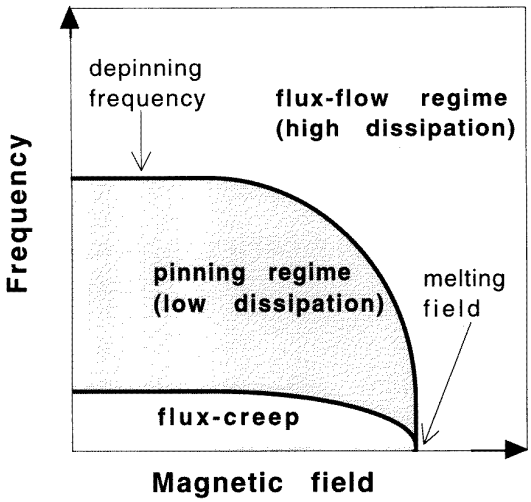

Figure 6. A schematic field–frequency diagram. In the pinning regime the vortex resistivity is primarily inductive and is determined by pinning. In the flux-flow regime the vortex resistivity is primarily resistive and is determined by viscosity, irrespective of whether vortices are pinned or unpinned. In the flux-creep (TAFF) regime the vortex resistivity is primarily resistive, although it is much smaller than in the flux-flow regime. The lines separating different regimes of the vortex dissipation are determined by the condition $\mathrm{Im}(\rho_v) = \mathrm{Re}(\rho_v)$ and do not necessarily coincide with phase transitions.

3.2. Vortex resistivity in the Hall regime

Since work is still in progress on the understanding of the high-frequency Hall effect in superconductors in the presence of pinning [1, 10, 12, 13, 30, 31] we will restrict the discussion to the case when only the viscous and the Hall term are relevant. The solution of equation (10) for $\boldsymbol{J} = \text{const}$ yields $v_x = J\Phi_0\eta/(\eta^2+\alpha_H^2)$, $v_y = J\Phi_0\alpha_H/(\eta^2+\alpha_H^2)$. The dissipation is $\sim \eta v^2/2 = (J\Phi_0)^2/2(\eta + \alpha_H^2/\eta)$. This yields the vortex resistivity

$$(\rho_v)_{xx} = \frac{B\Phi_0}{\eta + \alpha_H^2/\eta} = \frac{B\Phi_0}{\eta^*}. \tag{12}$$

Hence, an accounting for the Hall effect for $\boldsymbol{J} = \text{const}$ is equivalent to the substitution of η by an effective viscosity $\eta^* = \eta + \alpha_H^2/\eta$. Then equations (3*a*), (3*b*) and (4) yield

$$\eta^* = \pi\hbar n\omega_c\tau = \pi\hbar n\frac{\Delta E}{\delta E}. \tag{13}$$

Equation (13) is valid for all values of $\omega_c\tau$. It closely resembles the Bardeen–Stephen result (equation (2)) which was derived for $\omega_c\tau \ll 1$. It means that, due to the Hall effect, both the viscosity and the direction of the vortex motion are changed. However, when the dissipation for $\boldsymbol{J} = \text{const}$ is calculated, these two effects cancel out and the effective vortex viscosity is the same as if the Hall effect were absent. This cancellation takes place only for $\boldsymbol{J} = \text{const}$, when an external source drives a constant current through the superconductor with vortices. If the external source maintains constant voltage and not constant current, this cancellation does not take place.

3.3. Vortex resistivity in the flux-creep regime

Equation (10) may be solved analytically assuming a sinusoidal pinning potential with a peak-to-peak value U (see figure 3). The solution [24–26, 33] yields the vortex resistivity

$$\mathrm{Re}(\rho_v) = \frac{B\Phi_0}{\eta}\frac{\chi + (\omega/\omega_0)^2}{1 + (\omega/\omega_0)^2} \tag{14a}$$

$$\mathrm{Im}(\rho_v) = \frac{B\Phi_0}{\eta}\frac{(1-\chi)\omega/\omega_0}{1 + (\omega/\omega_0)^2} \tag{14b}$$

where

$$\omega_0 = \frac{k_p}{\eta}\frac{1}{1-\chi}\frac{I_1(\nu)}{I_0(\nu)}. \tag{14c}$$

Here, the flux-creep factor is $\chi = 1/I_0^2(\nu) < 1$, $\nu = U(T)/2kT$, $I_0(\nu)$ and $I_1(\nu)$ are modified Bessel functions. Analysis of equations (14) show that the flux creep increases $\mathrm{Re}(\rho_v)$, especially at low frequencies, and slightly decreases $\mathrm{Im}(\rho_v)$.

3.4. Nonlinearities

Equation (10) describes linear vortex dynamics. Nonlinear vortex dynamics may originate from several sources:

(i) Flux creep. Since the pinning potential strongly depends on current [1], the flux-creep factor is also current dependent, i.e. $\chi = \chi(J)$. Then, equation (14) yields a nonlinear vortex resistivity $\rho_v(J)$. This nonlinearity is very pronounced in the d.c. measurements, since the flux creep is the dominant source of d.c. resistivity in the superconducting state. However, this type of nonlinearity is not very important for high-frequency measurements, since the a.c. resistivity is determined mostly by viscous losses (factor $(\omega/\omega_0)^2$ in equation (14*a*)) and not only by the flux creep (χ factor in equation (14*a*)). As will be shown later, at $\omega/2\pi \gg 10^8$–10^9 Hz and at $T < 77$ K the flux-creep factor may be totally neglected in equation (14). Therefore, the nonlinearities related to flux creep are relatively unimportant in the microwave range.

(ii) Nonlinear response of pinned vortex. The parabolic approximation of the pinning potential is valid only for very small vortex displacements. At large vortex displacements the pinning force is no longer proportional to the displacement, and this may result in nonlinearity [34].

(iii) Sufficiently high current generates vortices. Therefore, vortex concentration depends on the current and vortex dynamics becomes nonlinear. This mechanism is especially important when the sample has a strip geometry, because high current concentration on the edges alleviates vortex generation [35–37].

(iv) Vortex motion under the action of an alternating current results in the spatial variation of magnetic induction. This variation, according to London equations, produces supercurrent (which depends on the vortex concentration) that enters the right-hand side of equation (10). This is an additional source of nonlinearity which was treated by Coffey [38].

(v) Vortex motion with high velocity leads to the non-equilibrium distribution of the quasiparticles in the vortex

core which results in the decrease of viscosity at high velocities. Larkin and Ovchinnikov [39] found

$$\eta(v) = \frac{\eta(0)}{1 + (v/v^*)^2} \tag{15}$$

where $v^*(T)$ is a characteristic velocity. Since $v \sim J$, equation (15) predicts a nonlinear resistance at low currents and an instability (at $v = v^*$) [40] at high currents.

4. Experimental determination of the dynamic vortex parameters

The vortex complex resistivity (equation (14)) is usually evaluated from the study of the surface impedance, Z. Typical measurements of Z include resonant methods [35–37, 41–63] microwave [64] or far-infrared [65, 66] transmission through thin films. Some information may be obtained from the nonlinear surface impedance in a high microwave field (rf-critical state) [35–37]. Viscosity may be measured in the free-flux-flow regime (which occurs at very high current densities) through the analysis of the d.c. I–V curves [40, 67, 68]. The Hall constant is measured either by using d.c. transport measurements [69] or through the Faraday effect upon transmission of submillimetre waves through thin superconducting films [65]. The pinning constant may be determined through the analysis of I–V curves [70], vibrating reed studies [71–73] a.c. susceptibility [20] and kinetic inductance of thin films [23, 24]. We will concentrate here on the surface impedance measurements (table 1). The advantage of this method is that the pinning constant and viscosity may be measured simultaneously on the same sample. This minimizes ambiguity in their determination.

5. Vortex dynamics from the complex impedance studies

5.1. Complex impedance of a superconductor in the mixed state. The Coffey–Clem model

The surface impedance Z is closely related to the complex penetration length λ

$$Z_s = R_s - iX_s = i\omega\mu_0\lambda. \tag{16}$$

Here R_s is the surface resistance and X_s is the surface reactance. The penetration depth is strongly dependent on magnetic field. This dependence comes mostly from vortices. Coffey and Clem [26] developed a model which describes the field dependence of the penetration length originating from the vortex mechanism. This model predicts

$$\lambda(B, T) = \left(\frac{\lambda_s^2 + \lambda_v^2}{1 + 2i\lambda_s^2/\delta_{nf}^2}\right)^{1/2}. \tag{17}$$

Here λ_s is the condensate penetration length, δ_{nf} is the normal-fluid skin depth and λ_v is the vortex penetration depth. The λ_v is directly related to the vortex resistivity ρ_v:

$$\lambda_v = \left(\frac{i\rho_v}{\omega\mu_0}\right)^{1/2}. \tag{18}$$

In most experiments the corrections for the quasiparticle skin depth and for the flux creep are important only close to T_c, so the high-frequency penetration depth in a magnetic field and at $T < T_c$ may be written as $\lambda^2(B, T) \approx \lambda_s^2(T) + \lambda_v^2(B, T)$. This means that the vortex and the condensate contributions are almost additive. From equations (14) and (18) we find the real and imaginary parts of λ_v:

$$\mathrm{Re}(\lambda_v^2) = \frac{\Phi_0 B}{\omega_0\eta\mu_0}\frac{1-\chi}{1+(\omega/\omega_0)^2} \tag{19a}$$

$$\mathrm{Im}(\lambda_v^2) = \frac{\Phi_0 B}{\omega_0\eta\mu_0}\frac{\omega/\omega_0}{1+(\omega/\omega_0)^2}\left[1 + \chi\left(\frac{\omega_0}{\omega}\right)^2\right] \tag{19b}$$

$$\frac{\mathrm{Im}(\lambda_v^2)}{\mathrm{Re}(\lambda_v^2)} = \frac{\omega}{\omega_0}\frac{1+\chi(\omega_0/\omega)^2}{1-\chi}. \tag{19c}$$

The complex penetration length is found from the experimentally measured surface resistance and surface reactance, using equation (16). The vortex dynamic parameters are obtained from the equations (17)–(19). Actually, there are three independent parameters, i.e. viscosity η, pinning constant k_p, and the flux-creep factor χ (ω_0 is related to them through equation (14*c*)). The unambiguous determination of these parameters requires measurement of the surface resistance and reactance at different frequencies. However, if the flux-creep factor is very small (as it is suggested in a large number of experiments), the measurements at one frequency are enough to find both η and k_p.

5.2. Complex impedance of a superconductor in the mixed state. Beyond the Coffey–Clem model

Most experimental data on the surface impedance of oxide superconductors in the mixed state are fairly well described by the Coffey–Clem model, using equations (17)–(19). However, this model has certain limitations as it does not account for the following effects:

(i) *Vortex lattice effects.* Since the Coffey–Clem model [26] is a continuous one (the length scales are given by λ), it does not account well for the situations in which the effects of the vortex lattice play the primary role and an additional length scale (intervortex spacing) appears. These cases include the a.c.-vortex Josephson effect (Fiory [74]) and the surface layer in a flat superconductor in a parallel magnetic field (Sonin *et al* [75]).

(ii) *Fluctuations close to* T_c. Since Coffey–Clem model uses a mean-field approximation, it is not expected to provide correct results in the fluctuation-dominated regions close to T_c or H_{c2}. Nevertheless, since equation (17) correctly accounts for the limiting cases of $T = T_c$ and $H = H_{c2}$, it may probably be applied in the fluctuation-dominated regions at least as an interpolation scheme. To find out the accuracy of such an interpolation, one should compare the prediction of the Coffey–Clem model for the field derivative of the surface resistance and reactance at $T = T_c$ and $H = H_{c2}$ with the results of microscopic theory. Such a theory was developed by Caroli and Maki

Table 1. Relevant experiments.

Reference	H (T)	Method	Material
Parks *et al* [65]	6	100–500 GHz pulse transmission	YBCO film 70 nm thick
Pambianchi *et al* [52]	0–0.35	11 GHz parallel-plate resonator	YBCO film 1 μm thick
Wu *et al* [28]	0–9	45 MHz–50 GHz Corbino disk	YBCO thin film
Owliaei *et al* [51]	0–8	10 GHz cavity resonator	YBCO thin film
Golosovsky *et al* [53]	0–0.8	5.5 GHz parallel-plate resonator	YBCO thin film
Ghosh *et al* [54]	0–7	11 GHz parallel-plate resonator	YBCO thin film
Revenaz *et al* [55]	0–6	1–20 GHz stripline resonator	YBCO thin film
Xavier *et al* [56]	0–7	5 MHz–5 GHz stripline	Ho–Ba–Cu–O thin film
Morgan *et al* [45]	4	27 GHz cavity resonator	YBCO single crystal
Matsuda *et al* [59]	0–6	30 GHz bolometry	YBCO single crystal
Wu and Sridhar [24]	0–0.02	6 MHz rf oscillator	YBCO single crystal
Hebard *et al* [23]	1–14	1.25 kHz kinetic inductance	YBCO thin film
Kunchur *et al* [68]	0–8	Pulsed d.c. current	YBCO thin film
Doettinger *et al* [40]	0–4	High d.c. current	YBCO thin film
Bulaevskii *et al* [114]		Reversible magnetization	BSCCO single crystal
Hanaguri *et al* [62]	2–5	44 MHz rf resonator	BSCCO single crystal

[76] and Thompson [77] (in the context of conventional superconductors) who found

$$\left(\frac{\partial R_s}{\partial H}\frac{H_{c2}}{R_n}\right)_{H_{c2}} = \frac{S(\omega,T)}{2} \approx 1\text{–}3 \qquad (20)$$

where R_n is the surface resistance in the normal state. It is not clear how close to this rigorous result are the predictions of the Coffey–Clem model.

(iii) *Vortex phase transition.* In the close vicinity to the vortex phase transition, the vortex dynamics is no longer described by the mean-field models such as equations (10) and (11). Indeed, Olsson *et al* [41], Wu *et al* [42], Ando *et al* [43], Yeh *et al* [44], Koetzler *et al* [78] and Wu *et al* [28] experimentally found a dramatic change in the high-frequency vortex dynamics across the vortex phase transition. It was found that the scaling model of Fisher *et al* [79] fairly well accounts for the transition region. If one tries to describe this region in terms of vortex viscosity and pinning constant [43] these parameters acquire frequency dependence. Wu *et al* [28] have recently demonstrated that the scaling models work better at low frequencies, $\omega/2\pi < 10$–20 GHz, while at higher frequencies the mean-field models of equations (10) and (11) are still applicable.

Giura *et al* [80] and Sarti *et al* [81] have recently developed a procedure which accounts for the temperature-dependent d.c. resistivity of superconductors in a magnetic field through phase transition (both superconducting and vortex liquid–vortex solid). It is highly desirable to develop a similar procedure for the a.c. resistivity, since it has importance for applied superconductivity. Indeed, magnetic-field-modulated microwave absorption (MAMMA) has evolved as a valuable tool for the search of new superconducting compounds [82–84]. This method consists of measuring the field derivative of the surface resistance of superconductor at varying temperature. A sharp peak in dR_s/dH appears at T_c which permits T_c to be established with high accuracy. This method is contactless, very sensitive, and is widely used with the commercial 10 GHz ESR equipment. As far as we know, there is no satisfactory model that describes the peak. If such a model were present, the MAMMA measurements would yield not only a T_c value, but additional information characterizing the quality and properties of the superconducting samples.

6. Experimental studies of the complex impedance

Typical complex impedance studies include measurement of the magnetic-field-dependent Q-factor and the resonant frequency of a microwave resonator with superconductor. A superconductor may (i) be mounted inside a copper resonant cavity [45–49], (ii) serve as an end-plate of a copper cavity [50, 51], (iii) form a resonator by itself (parallel-plate resonator [52–54], microstripline [55–57], dielectric resonator [44]), (iv) terminate a coaxial cable [58]. Viscosity (but not the pinning constant!) may be estimated from the study of the surface resistance in a magnetic field by the bolometric technique [59, 60]. In the radio-frequency range the sample is mounted in the rf coil and its complex impedance is yielded from the a.c. magnetic susceptibility [24, 61, 62].

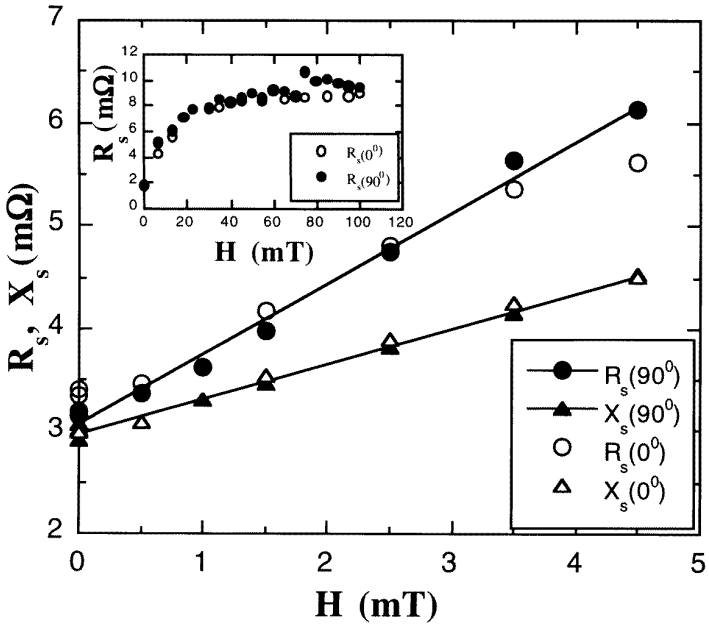

Figure 7. Magnetic-field dependence of the surface resistance R_s and reactance X_s of a pair of laser-ablated $YBa_2Cu_3O_7$ films with weak links [86]. Θ is the angle between the field and the *c*-axis. Note the linear dependence at low field and saturation at higher fields (inset). T = 57 K, f = 5.4 GHz, $\boldsymbol{H} \perp \boldsymbol{j}$.

6.1. Vortices versus weak links

An important point in the study of vortex dynamics is to make sure that the magnetic field effect on the surface impedance and penetration length originates from the vortices and not from other sources, such as weak links or pair breaking. The pair-breaking mechanism in oxide superconductors has been extensively studied by Wu and Sridhar [24] and Maeda *et al* [61]. It is dominant at $H < H_{c1}$ and negligible at higher fields. As to the weak links, their contribution at certain conditions may dominate over that of the vortices. This frequently occurs at low field values $\mu_0 H < 0.1$ T. The weak-link contribution may be recognized through its nonlinear behaviour [35, 36, 63, 85], field, angular and temperature dependence [86], which are very different from those for the vortex mechanism. Indeed, R_s and X_s of the films containing weak links increase linearly with increasing field (figure 7) and saturate at low field $\mu_0 H \approx 0.1$ T (figure 7, inset), while for the vortex mechanism the saturation (if any!) occurs at higher fields [51, 58]. The angular dependence of the surface impedance, arising from the weak-link mechanism, may be negligible (figure 7), while for the vortex mechanism it is very pronounced. For example, figure 8 demonstrates the field dependence of the surface resistance and reactance of a pair of $YBa_2Cu_3O_7$ films [53] free of weak links. Both R_s and X_s increase with increasing field. The effect of the magnetic field is the strongest when $\boldsymbol{H} \| \boldsymbol{c}$ ($\Theta = 0^\circ$) and the weakest when $\boldsymbol{H} \perp \boldsymbol{c}$ ($\Theta = 90^\circ$).

6.2. Flux creep

The activation energy for the flux creep may be found from the d.c. magnetization studies. Abulafia *et al* [87] (local probe) and Schalk *et al* [88] have demonstrated that the pinning potential in $YBa_2Cu_3O_7$ has a pronounced temperature dependence. This dependence is different at high and low temperatures. At low temperatures ($T <$ 70 K) [87, 88] find $U \propto kT$ and $U/2kT = \nu \approx 6.5$–9. These results suggest a very small and temperature-independent flux-creep factor (see section 3.3), namely $\chi \approx 10^{-6}$–10^{-4}. It means that the effect of the flux creep on the depinning frequency ω_0 (equation (14*c*)) and on the imaginary part of the vortex resistivity (equation (14*b*)) should be negligible at all frequencies, while the effect of the flux creep on the real part of the vortex resistivity (equation (14*a*)) should be negligible only at high frequencies, $\omega \gg \omega_0 \chi^{1/2}$. We will show later that the depinning frequency in $YBa_2Cu_3O_7$ is $\omega_0/2\pi \approx 10^{10}$–$10^{11}$ Hz. Hence, the d.c. magnetization data suggest that in the frequency range $\omega/2\pi \gg 10^8$–10^9 Hz, the flux-creep factor may be totally neglected in equations (14). The estimates of the flux-creep factor from the surface impedance studies well agree with the conclusions drawn from the d.c. magnetization studies. Indeed, Revenaz *et al* [55], using swept frequency studies, estimated the flux-creep pinning energy at 4.2 K as $U/2kT = \nu \approx 4.8$–6.5 (this corresponds to the flux-creep factor of $\chi \approx 10^{-3}$–10^{-4}). Parks *et al* [65] demonstrated that the flux-creep factor is unimportant at very high frequencies $\omega/2\pi >$ 100 GHz.

In the high-temperature range ($T >$ 70 K), the d.c. magnetization data [88] suggest that the pinning potential acquires a different temperature dependence and becomes small. This suggests a non-negligible flux-creep factor close to T_c. Indeed, the swept-frequency studies of Wu *et al* [28] yielded a non-negligible flux-creep factor $0.05 < \chi < 0.5$ at 80 K $< T <$ 86 K.

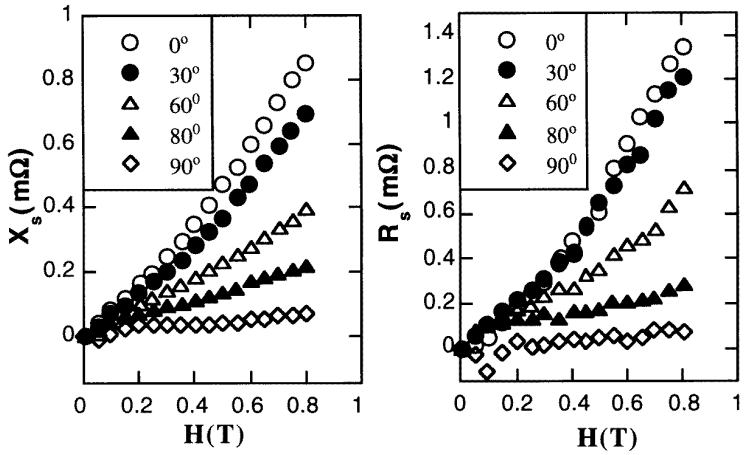

Figure 8. Magnetic field dependence of the surface resistance R_s and surface reactance X_s of laser-ablated $YBa_2Cu_3O_7$ films at different angles [53]. Θ is the angle between the field and the c-axis. T = 57 K, f = 5.4 GHz, $\boldsymbol{H} \perp \boldsymbol{j}$. Only the field-dependent parts of R_s and X_s are shown.

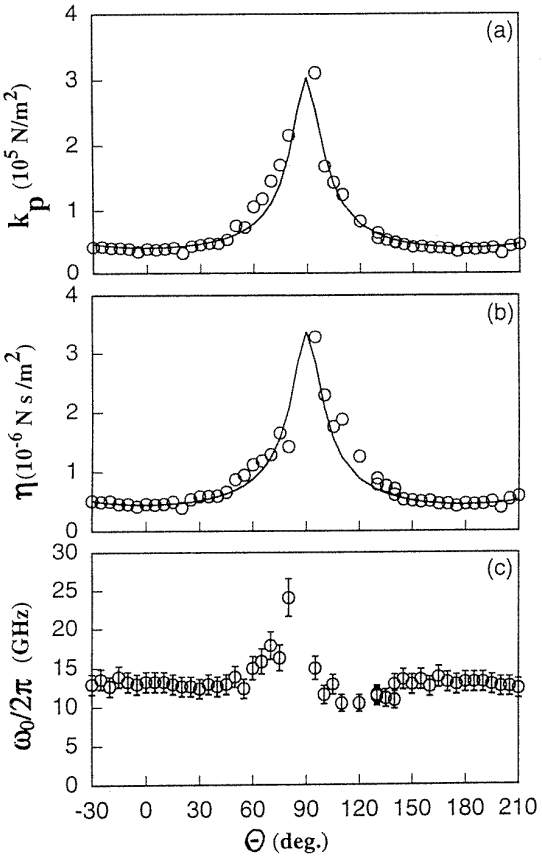

Figure 9. Angular dependence of the pinning constant k_p, viscosity η and depinning frequency $\omega_0/2\pi$ at T = 57 K and 0.1 T < B < 0.8 T. Θ is the angle between the field and the c-axis. The full curves show approximations $k_p(\Theta) = k_p(0^\circ)/\varepsilon_\Theta$, $\eta(\Theta) = \eta(0^\circ)/\varepsilon_\Theta$, $\varepsilon_\Theta = (\cos^2\Theta + \gamma^{-2}\sin^2\Theta)^{1/2}$ and γ = 7.5.

6.3. Field dependence of the pinning constant, viscosity and depinning frequency

The majority of high-frequency studies in $YBa_2Cu_3O_7$ yield field-independent η and k_p. Namely, a field-independent pinning constant was found for: (table 1) (i) $Bi_2Sr_2CaCu_2O_8$ single crystal [62] at $T > 25$ K and $\mu_0 H < 2$ T; (ii) for $YBa_2Cu_3O_7$ thin films for $\mu_0 H < 0.8$ T [53], for $\mu_0 H < 14$ T [23], and for $\mu_0 H < 6$ T [55]. These results suggest individual vortex pinning over a wide range of fields and temperatures. This is very different from conventional superconductors, in which the pinning is usually collective and $k_p \sim B^{-1/2}$ [21]. Of course, the vortices in $YBa_2Cu_3O_7$ should enter the collective pinning regime upon increasing field (and the pinning constant should acquire field dependence). Indeed, at high fields and high temperatures a dramatic change in the vortex electrodynamics occurs. This was observed by Owliaei *et al* [51], Wu *et al* [42], Booth *et al* [58] and Thrane *et al* [89]. This transition occurs approximately at the irreversibility line [51, 89]. Therefore, it was interpreted as a glass transition [51, 58, 89] rather than transition to the collective pinning regime.

6.4. Angular dependence of the surface impedance

6.4.1. Lorentz force. The angular dependence of the surface impedance may originate from: (i) the angular dependence of the Lorentz force, (ii) geometrical factors [90, 91] and (iii) anisotropy of the vortex dynamic parameters (which results from the crystal anisotropy). The Lorentz force-induced anisotropy appears in those experiments, in which the direction of the field is changed relative to that of the current. Studies of the angular dependence of the surface impedance in conventional (isotropic) superconductors revealed the angular dependence appropriate to the Lorentz force [92]. Similar experiments in granular $YBa_2Cu_3O_7$ films [64] and ceramics [48] demonstrated the angular dependence of the vortex resistivity, which was consistent with the Lorentz force (although in both experiments there was an appreciable isotropic background). Recent microwave experiments of Ghosh *et al* [54] on epitaxial films proved the angular dependence characteristic for the Lorentz force, i.e. the field effect on the surface resistance and reactance

was much stronger in the geometry when the field was perpendicular to the current than in the parallel geometry.

6.4.2. Angular dependence of the pinning constant, viscosity and depinning frequency. The angular dependence of R_s and X_s, arising from the anisotropy of the viscosity and pinning constant, is probed in those experiments in which direction of the field is changed relative to the crystal axis so that $\boldsymbol{H} \perp \boldsymbol{j}$. Figure 9 shows the angular dependences of k_p, η and ω_0 found in such an experiment. We note that the angular dependences of k_p and η are very similar, while ω_0 is almost independent of angle. The viscosity and the pinning constant exhibit maximum values when $H \perp c$ and minimum values when $H \| c$. The anisotropy of the pinning constant is $\gamma = k_{p\perp}/k_{p\|} \approx 7.5$. Anand and Tinkham [57] have found a similar anisotropy of the surface resistance of thin films ($\gamma = 7$–8) for $\mu_0 H = 0.05$ T and an enhanced anisotropy ($\gamma = 15$) for lower field values such as $\mu_0 H = 0.01$ T. The study of the field-modulated microwave absorption across T_c in single crystals (which is determined by both η and k_p) [49] yields $\gamma = 6.7$. These values of γ are approximately consistent with the effective mass anisotropy of $YBa_2Cu_3O_7$, $(m_c/m_{ab})^{1/2} = 5$–8. In contrast to these results, an analysis of the I–V curves [93] yields a much lower anisotropy, $k_{p\perp}/k_{p\|} = 1.7$. Moreover, Wu and Sridhar [24] find inverse anisotropy of the pinning constant for the $YBa_2Cu_3O_7$ single crystals, namely $k_{p\|}/k_{p\perp} = 0.1$. This last result is definitely different from other results. It may originate from the fact that the experiments in [24] were performed at low field values, such as $\mu_0 H \leq 0.1$ T, $H \approx H_{c1}$, while other data [53, 57] were collected at a higher field $\mu_0 H \leq 1$ T, $H \gg H_{c1}$. Also, the pinning mechanism at low fields may be different from that at higher fields (for example, the low-field pinning constant may be determined by surface barriers [94]). Actually, γ may be temperature dependent due to competition between 3D and 2D behaviour [95].

6.4.3. Scaling approach. The angular dependence of the pinning constant and viscosity (figure 9) is in good agreement with scaling models [96–99]. Such models map the angular-dependent properties of a uniaxial anisotropic superconductor in the mixed state ($H_{c1} \ll H \ll H_{c2}$) to the isotropic case by replacing the magnetic field at an arbitrary angle Θ by a reduced field $b = B\varepsilon_\Theta$ (where $\varepsilon_\Theta = (\cos^2\Theta + \gamma^{-2}\sin^2\Theta)^{1/2}$). We recast equation (19) (assuming $\chi \to 0$) and find

$$\lambda_v^2(B,\Theta) = \lambda_v^2(b) = \frac{b\Phi_0}{\mu_0 k_p(b)[1 - i(\omega/\omega_0'(b))]}. \qquad (21)$$

Here $k_p(b) = k_p(B, 0^\circ)$ and $\omega_0'(b) = \omega_0(B, 0^\circ)$. The experiment [53] yields $\lambda_v^2(B, 0^\circ) \sim B$. Then equation (19) yields $\lambda_v^2(b) \sim b/k_p$ where k_p is field independent. Therefore, $\lambda_v^2(B,\Theta) \sim B\varepsilon_\Theta/k_p(0^\circ)$, and $k_p(\Theta) = k_p(0^\circ)/\varepsilon_\Theta$. In the same way we find $\eta(\Theta) = \eta(0^\circ)/\varepsilon_\Theta$. Of course, equation (21) does not work if the pinning itself is anisotropic, for example if it is achieved by preferentially oriented twin-boundaries, columnar defects or by internal pinning [100]. Indeed, Lofland *et al* [101] have observed that introduction of columnar defects dramatically changes the angular dependence of the field-modulated microwave absorption.

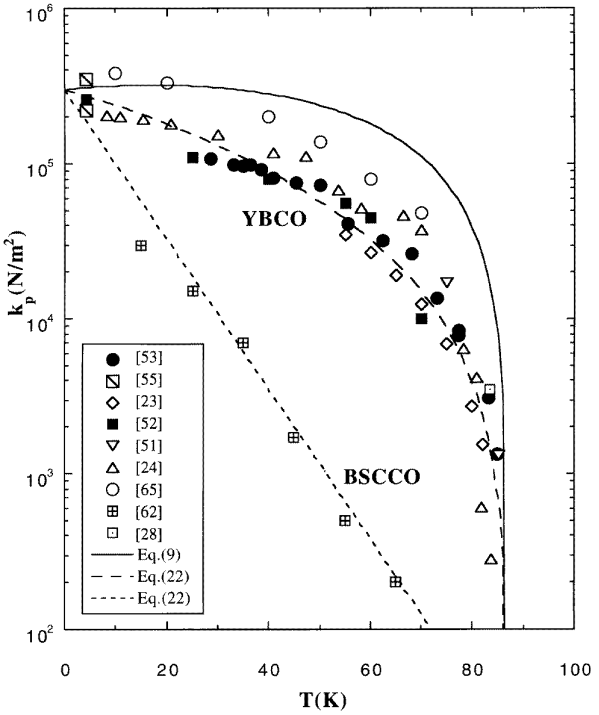

Figure 10. Temperature dependence of the pinning constant k_p in the regime of individual pinning (field-independent pinning constant). The full curve demonstrates an approximation $k_p(T) = k_p(0)(1-t)^{4/3}(1+t)^2$ with $T_c = 88$ K and $k_p(0) = 3 \times 10^5$ N m^{-2}. The broken lines show exponential dependences $k_p(t) = k_p(0)(1-t)^{4/3}(1+t)^2\exp(-T/T_0)$ with the same T_c and $k_p(0)$. Fluctuation-dependent temperatures are $T_0 = 28$ K for $YBa_2Cu_3O_7$ and $T_0 = 9$ K for $Bi_2Sr_2CaCu_2O_8$.

6.5. Temperature dependence

6.5.1. Pinning constant. Figure 10 demonstrates the temperature dependence of the pinning constant for thin films and single crystals as measured by electrodynamic methods. Clearly, the low-temperature values of k_p are very high, of the order of $\mu_0 H_c^2(0)$. The following question arises: if k_p in $YBa_2Cu_3O_7$ is so high, why is the critical current J_c not very high, and why is the pinning energy U so low? This point was analysed several years ago by Hylton and Beasley [102] with the emphasis on critical current. The answer is related to the very short-range pinning potential (which originates from the very short coherence length [103]). Indeed, let r_p be the radius of the action of the pinning potential, then $J_c \approx k_p r_p$ and $U \approx k_p r_p^2$. While k_p is large, r_p is small. Hence, in spite of high k_p values, both J_c and U are small.

We compare the zero-temperature value of the pinning constant with that given by equation (9). Since $\mu_0 H_c(0) = 1.2$ T [104], equation (10) yields $(k_p(0))_{max} = (1$–$6) \times 10^4$ N m^{-2}. The experimental values of the pinning

constant for most of the samples (except ceramics!) are several times bigger, namely $(k_p(0))_{\text{experiment}} = (20\text{–}40) \times 10^4$ N m^{-2}. This is surprising, since we would expect the experimental value of the pinning constant to be *smaller* than the maximum pinning constant! What is the possible source of the discrepancy? A probable explanation is that the line tension e_l (equation (7)) is bigger. Some indication of it is given in the work of Liang *et al* [105] who estimated the line energy from the data on the penetration length λ and H_{c1} of a $YBa_2Cu_3O_7$ single crystal and found that the line energy is three times bigger than that given by equation (7).

Apart from giving too low a value of the zero-temperature pinning constant $k_p(0)$, equation (9) does not provide a satisfactory fit for the temperature dependence of the pinning constant, as is demonstrated in figure 10 (full line). A much more satisfactory fit is provided by an extension of the same model that takes into account smearing of the pinning potential by thermal fluctuations [1, 106]. According to this model, the modified pinning potential is

$$U(T) = U_0(T) \exp(-T/T_0). \tag{22}$$

Here $U_0(T)$ is the temperature-dependent pinning potential without thermal fluctuations (the dependence on T originates from the temperature dependence of the superconducting parameters, such as condensation energy) and T_0 is a characteristic temperature, that depends on fluctuations. In the limit $T_0 \ll T_c$ the temperature dependence of the pinning potential is dominated by thermal fluctuations (exponential term in equation (22)), while in the opposite limit $T_0 \leq T_c$, thermal fluctuations are unimportant. Since $k_p = \mathrm{d}^2U/\mathrm{d}x^2$ and $J_c \sim \mathrm{d}U/\mathrm{d}x$, their temperature dependence is also expected to be exponential. Indeed, such exponential dependence with $T_0 \approx 17$–25 K was observed for the critical current [107, 108] and in vibrating-reed studies [73] in $YBa_2Cu_3O_7$ single crystals. We apply this model [1, 106] to the pinning constant and assume that the value given by equation (9) should be multiplied by the factor $\exp(-T/T_0)$. Indeed, the experimental data for $YBa_2Cu_3O_7$ are satisfactorily described by such a dependence with $T_0 \approx 28$–35 K (figure 10 broken line). The model [1, 106] predicts that the fluctuation-induced smearing of the pinning potential should be much more pronounced in $Bi_2Sr_2CaCu_2O_8$ due to the enhanced anisotropy. Indeed, while the low-temperature pinning constant of a $Bi_2Sr_2CaCu_2O_8$ single crystal (extrapolation from the data of Hanaguri *et al* [62] to zero temperature) is almost the same as in $YBa_2Cu_3O_7$, it exponentially decreases at higher temperatures (figure 10).

The pinning constant of thin films and single crystals (figure 10) is several orders of magnitude higher than that of ceramics [24]. We find also (in contrast to Ziese *et al* [71]) that the pinning constant in thin films and single crystals, as measured electrodynamically (figure 10), is considerably higher than that measured by the vibrating-reed method [71]. (Hence, a comparison of the pinning constants measured by both methods on the same sample is strongly desirable.) Another remarkable feature of figure 10 is that the values of the pinning constant obtained by various electrodynamic methods and with different $YBa_2Cu_3O_7$ materials are very close despite the enormous differences in the measuring frequency (1 kHz–500 GHz) and magnetic field (0.1–14 T). We can now discuss several possible explanations for this fact:

(i) The same defect determines the pinning constant in the majority of the samples. It may be, for example, oxygen vacancies or dislocations. Pinning by these defects was calculated by Kes [109]. However, to account for a very large value of the low-temperature pinning constant, this explanation requires a very high concentration of vacancies.

(ii) The pinning constant is determined not only by the interaction with the pinning sites, but by the short-range vortex elasticity as well (see figure 4). While the interaction with pinning sites may vary from sample to sample, the vortex elasticity is an intrinsic property of the material and the only parameter that introduces a difference between different samples is the density of the pinning sites. In this case the temperature dependence of the pinning constant in different samples should be the same, while its magnitude may differ. According to this scenario, the pinning sites in the samples shown in figure 10 are so strong that the pinning constant in all these samples is determined by the vortex elasticity. However, in ceramic samples [24] the pinning sites are weak and the pinning constant is determined by the interaction with the pinning sites.

(iii) Parks *et al* [65] argue that a strongly anisotropic gap may have a profound effect on the field dependence of the penetration depth. Actually, Parks *et al* assume that the magnetic-field-induced inductive response in $YBa_2Cu_3O_7$ arises from the pair breaking and not from the pinning. One difficulty with this explanation is that it suggests the field-dependent pinning constant, i.e. $k_p \sim B^{1/2}$, while most experiments (table 1) yield a field-independent k_p. Another difficulty is the assumption that the pinning response is completely masked by the pair-breaking response. Indeed, Parks *et al* assume that $k_{\text{electrodynamic}} = 1/(1/k_{\text{pair breaking}} + 1/k_{\text{pinning}})$ and $k_{\text{electrodynamic}} \approx k_{\text{pair breaking}} \ll k_{\text{pinning}}$. Therefore, the electrodynamic experiments probe pair breaking, while the actual pinning constant should appear in vibrating-reed studies. However, the pinning constant values, as found in vibrating-reed studies [71], are systematically lower than those found in the electrodynamic studies, not higher! This is in contradiction to the conjecture of Parks *et al* [65].

6.5.2. Viscosity. Figure 11 shows experimental viscosity values at $T > 70$ K. We observe that the values obtained by the high-frequency methods are in reasonable agreement with those obtained from the d.c. studies. We compare viscosity values with the predictions of the microscopic theory of Gorkov and Kopnin [17] for the flux-flow resistance at low fields, $H \ll H_{c2}$. This theory predicts $\rho_{ff} = \rho_n B/\beta\mu_0 H_{c2}(t)$, where β is a dimensionless slowly varying function of temperature. Since in the vicinity of T_c the critical field linearly depends on temperature, i.e. $H_{c2}(t) \sim 1 - t$, then

$$\eta(T) = \frac{\beta(t)(1-t)\mu_0\Phi_0}{\rho_n}\left(\frac{\mathrm{d}H_{c2}}{\mathrm{d}t}\right)_{T_c}. \tag{23}$$

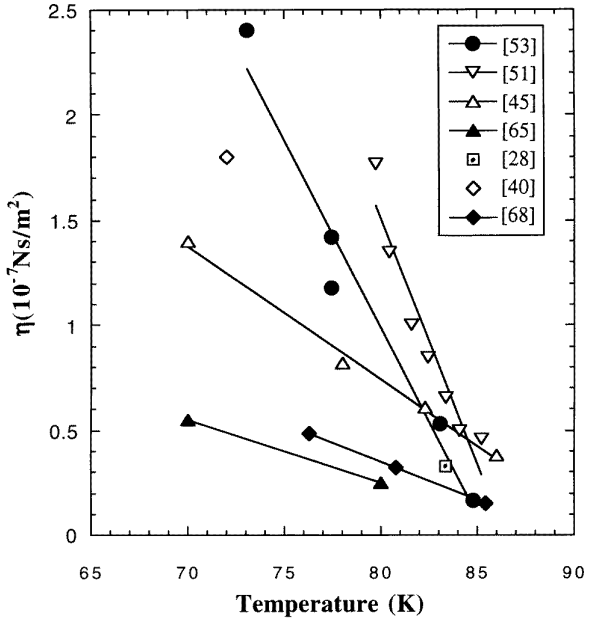

Figure 11. Temperature dependence of the viscosity in $YBa_2Cu_3O_7$ in the vicinity of T_c. Full lines show linear approximations $\eta(t) \sim 1 - t$. Note that the data of [45, 51, 53, 65, 68] are obtained by high-frequency methods while the data of [28, 40] are found in d.c. measurements.

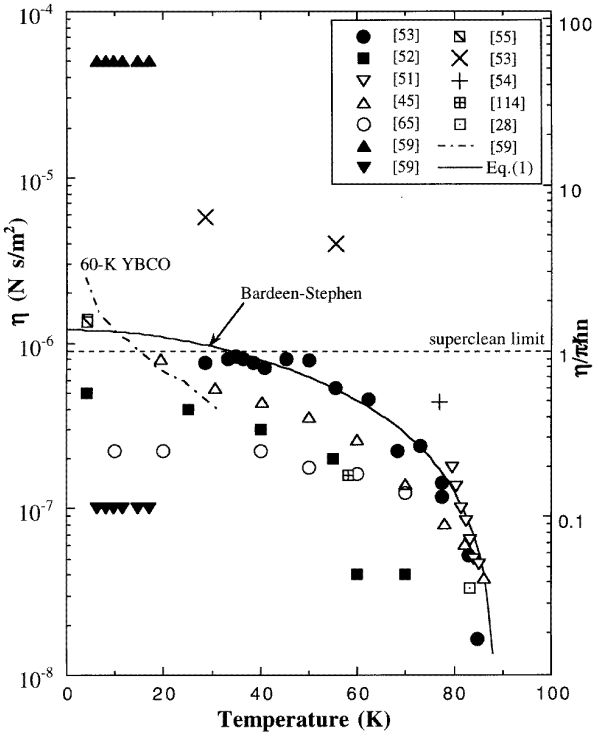

Figure 12. Temperature dependence of the viscosity in $YBa_2Cu_3O_7$. Open and full symbols show the data for $H \| c$. Crosses show the data for $H \perp c$. Full triangles show the data of Matsuda *et al* [59]. Full inverted triangles show reconsidered data of Matsuda *et al* [59] (see text). The chain curve shows the data of Matsuda *et al* [59] for the 60 K $YBa_2Cu_3O_7$. The full curve shows an approximation $\eta(T) = \eta(0)(1 - t^2)/(1 + t^2)$ with $T_c = 88$ K and $\eta(0) = 1.2 \times 10^{-6}$ N s m^{-2}. The broken line shows the superclean limit.

Figure 11 demonstrates that viscosity is, indeed, linearly dependent on $1 - t$. Taking $\rho_n = 70$ $\mu\Omega$ cm, and $\mu_0\, dH_{c2}/dT = 1.9\ T/K$ [110], we find that the data for different groups yield β values ranging from 0.5 to 4. This should be compared with the $\beta = 2$–3 which is found in similar experiments on conventional superconductors [17].

Figure 12 shows the temperature dependence of the viscosity of Abrikosov vortices in $YBa_2Cu_3O_7$ in the whole temperature range. For the majority of the experiments, the low-temperature ($T < 77$ K) viscosity is in the limits $\eta = 10^{-7}$–10^{-6} N s m^{-2}. This value is several orders of magnitude higher than the viscosity of Josephson vortices (as measured by de Nivelle *et al* [111] at 4.2 K, namely $\eta_J \approx 10^{-10}$ N s m^{-2}). We note that almost all viscosity data, as measured by different techniques and for different samples, are spread within one order of magnitude (at each particular temperature). This spread may be related to the spread of the quasiparticle scattering time τ (equation (2)). However, the single-crystal data of Matsuda *et al* [59] are very different from other results. We note that the viscosity values reported by Matsuda *et al*, were obtained from the measurements of R_s at a single frequency $\omega/2\pi = 30$ GHz assuming that the depinning frequency is much lower than the measuring frequency. Now it is clear that the depinning frequency may be much higher [65], hence the initial assumption of negligible pinning made in [59] may be reconsidered. Since pinning constants for different samples do not differ much (figure 10), we reconsider the data of [59] assuming a pinning constant $k_p(0) = 4 \times 10^5$ N m^{-2}. We find that the surface resistance data of [59] may yield either $\eta = 5 \times 10^{-5}$ N s m^{-2} (which is almost two orders of magnitude higher than the values reported by other groups), or $\eta = 1 \times 10^{-7}$ N s m^{-2} (which is a rather small value, but it is closer to the results of other groups).

The Bardeen–Stephen expression for viscosity (equation (1)) may be inverted in order to calculate ρ_n at low temperatures. This procedure was proposed first by Morgan *et al* [45] and it yields the quasiparticle relaxation rate in the vortex core, $\tau^{-1}(T) = \tau^{-1}(T_c)\Phi_0\mu_0 H_{c2}(T)/\rho_n(T_c)\eta(T)$. The vortex relaxation rate $\tau^{-1}(T)$ was found to decrease in the superconducting state [45, 51, 52, 65]. In general, this decrease is consistent with the linear extrapolation of the normal-state resistivity below T_c [45]. This is very different from the exponential temperature decrease of the bulk relaxation rate $\tau_b^{-1}(T)$ [112], which was found from the analysis of the surface impedance in the absence of magnetic field.

6.5.3. Superclean limit. The superclean limit is achieved provided that the ratio of the level spacing $\Delta E = \Delta^2/E_F$ to the level width $\delta E = \hbar/\tau$ in the vortex core is higher than unity. Equation (13) demonstrate that this ratio may be directly determined from the viscosity value. Following Harris *et al* [69], we perform this estimate. It is important to note that most viscosity measurements by the surface impedance technique (figure 12) are done using undercoupled resonators (i.e. in the constant-current

mode). Equation (12) states that such measurements yield the vortex resistivity and not conductivity. If the Hall effect is taken into account, then the viscosity found in such measurements is not the actual viscosity η (equation (3*a*)) but the effective one η^* (equation (13)). In other words, figure 12 plots η^* and not η. The superclean limit is achieved provided $\omega_c\tau = \eta^*/\pi\overline{h}n > 1$. The y axis on the right-hand side of figure 12 shows $\eta^*/\pi\overline{h}n$. We assume that $n = 0.5$ carrier per unit cell [113] and that n is independent of the vortex orientation. We observe that the low-temperature data for $H \| c$ suggest $\eta^*/\pi\overline{h}n = \omega_c\tau \approx 0.1$–2. This should be compared with the value $\omega_c\tau = 2.2$ found in the infrared transmission experiments of Karrai *et al* [66]. We conclude that for $H \| c$ the vortices in 90 K $YBa_2Cu_3O_7$ (and in 60 K $YBa_2Cu_3O_7$ as well [69]) are close to or in the superclean limit. Since viscosity is considerably higher for $H \perp c$, we are forced to conclude that the vortices in the *a*–*b* planes are deep in the superclean limit! However, in order to make a firm conclusion, several precautions are needed. Indeed, the estimate of the parameter $\omega_c\tau$ from the magnitude of viscosity is based on equations (2) and (13) which assume a hydrodynamic limit, i.e. $\omega_c\tau \ll 1$. If such an estimate yields $\omega_c\tau \ll 1$, the procedure is self-consistent and the magnitude of $\omega_c\tau$ is reliable. However, if such an estimate yields $\omega_c\tau \gg 1$, this should be interpreted only as an indication of the superclean limit. No reliable estimate of the magnitude of $\omega_c\tau$ may be made yet because the whole procedure is not self-consistent. A detailed model of the vortex viscosity in the superclean limit is required. This model should address the following issues:

(i) *Anisotropy*. High viscosity values that are found for the vortex motion perpendicular to the CuO sheets may be considerably affected by the anisotropy of $YBa_2Cu_3O_7$. However, equations (2) and (5) do not explicitly account for anisotropy.

(ii) *Pinning*. The estimate of the superclean parameter $\omega_c\tau$ is based on equations (2), (5) and (13). These equations are obtained assuming negligible pinning, while most of the data plotted in figure 12 were obtained in the pinning regime.

(iii) *Low temperatures*. In the superclean limit and at very low temperatures $\Delta^2/E_F \gg kT$, the dissipation inside the vortex may be additionally hampered due to selection rules for momentum transfer between bound states [18]. This regime may be relevant for $YBa_2Cu_3O_7$, since $\Delta^2/E_F \sim 100$ K [66].

(iv) *Localization*. A vortex in the superclean limit is similar to a quantum wire in which one-dimensional localization of the quasiparticles may occur. This may have a profound effect on the dissipation of the moving vortex.

6.5.4. Hall constant. Viscosity data imply that the vortices in $YBa_2Cu_3O_7$ are close to the superclean limit. This means that the Hall effect may be observable, since equation (3*c*) yields an appreciable Hall angle, $\tan\Theta_H = \omega_c\tau \sim 1$. A big Hall effect was, indeed, observed in 60 K $YBa_2Cu_3O_7$ [69]. The Hall angle may be also estimated from the viscosity measurements, as it was done by Harris *et al* [69] in the context of 60 K $YBa_2Cu_3O_7$. Following their procedure we analyse the data of Parks *et al* [65] for the 90 K $YBa_2Cu_3O_7$ which reports $\eta(4.2\text{ K}) = (1.2\text{–}1.5) \times 10^{-7}$ N s m^{-2}. According to equations (3*a*) and (13) this implies $\omega_c\tau = 0.14$–0.17. Then equation (3*b*) yields the Hall constant $\alpha_H = (0.02\text{–}0.03)\pi n\overline{h}$ (assuming $n = 0.5$ carriers per unit cell). This value is only two to three times smaller than the experimental one [65], namely $\alpha_H = 0.07\pi n\overline{h}$. We conclude that while the d.c. measurements of the Hall effect in $YBa_2Cu_3O_7$ at low temperatures are hindered due to strong pinning, the high-frequency measurements may provide direct access to the Hall effect.

6.5.5. Depinning frequency. Figure 13 shows experimental values of the depinning frequency. We observe that the temperature dependence of the depinning frequency is not very strong, at least at $T/T_c < 0.8$. (Close to T_c the flux creep becomes dominant and depinning frequency loses its meaning). A useful insight into the physical meaning of the depinning frequency $\omega_0 = k_p/\eta$ may be obtained using the Bardeen–Stephen expression for the viscosity (equation (1)), and equation (6) for the maximum core pinning

$$\omega_0 \sim \frac{k_p}{k_p^{max}}\frac{n_s}{n}\tau^{-1}. \tag{24}$$

Here τ^{-1} is the quasiparticle relaxation rate in the vortex core, $n_s(t)$ is the concentration of Cooper pairs and n is the carrier concentration in the normal state. Equation (24) shows that the temperature dependence of ω_0 arises from the interplay between the temperature dependences of k_p/k_p^{max}, τ^{-1} and n_s. Since these dependences partly compensate one another, the temperature dependence of ω_0 is weak. At low temperatures, $n_s = n$. Hence, $\omega_0(T = 0) \approx (k_p/k_p^{max})\tau^{-1}$. The relaxation rate does not differ much for high-T_c and for conventional superconductors, while the pinning does differ (for high-T_c superconductors $k_p/k_p^{max} \sim 1$ while for conventional superconductors $k_p/k_p^{max} \ll 1$). Hence, the high values of depinning frequency in oxide superconductors are due to strong pinning.

7. Conclusions

(i) The values of the pinning constant reported by different researchers and for different $YBa_2Cu_3O_7$ samples show surprisingly small dispersion. The pinning constant at lowest temperatures is very high and decreases exponentially with increasing temperature. This suggests a pronounced effect of thermal fluctuations on pinning.

(ii) The measured viscosity values indicate that, at least at low temperatures, the vortices in $YBa_2Cu_3O_7$ may be in the superclean limit, i.e. there are bound states inside the vortex core. The values of the level spacing and level width, as given by viscosity measurements, are consistent with those found from the studies of Hall effect and infrared transmission.

(iii) The depinning frequency in $YBa_2Cu_3O_7$ thin films is almost independent of temperature and orientation and is of the order of 10–200 GHz. These values are considerably higher than those for conventional superconductors due to stronger pinning.

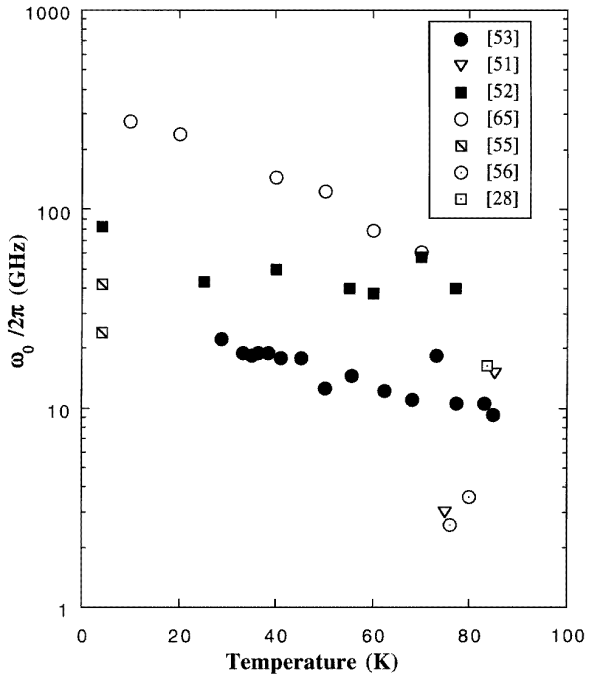

Figure 13. Temperature dependence of the depinning frequency.

Acknowledgments

We are grateful to V B Geshkenbein, V M Vinokur, J Orenstein, P Monod, N Bontemps, B Laikhtman, B Placais and I Yeshurun for useful discussions and to E B Sonin for crictical reading of the manuscript. This work was supported by the Israeli Ministry of Science and Arts, the European Community, the Klatchky foundation and the French–Israeli cooperation ('Arc en Ciel' program).

References

[1] Blatter G, Feigel'man M V, Geshkenbein V B, Larkin A I and Vinokur V M 1994 *Rev. Mod. Phys.* **66** 1147
[2] Brandt E H 1992 *Physica* C **195** 1
[3] Huse D A, Fisher M P A and Fisher D S 1992 *Nature* **358** 553
[4] Tinkham M 1980 *Introduction to Superconductivity* (New York: Krieger)
[5] Berkovits R and Shapiro B Ya 1995 *Phys. Rev.* B **51** 3151
[6] Caroli C, de Gennes P G and Matricon J 1964 *Phys. Lett.* **9** 307
[7] Kopnin N B and Kravtsov V E 1976 *JETP Lett.* **23** 578; (1976 *Pis'ma Zh. Eksp. Teor. Fiz.* **23** 631)
Kopnin N B and Salomaa M M 1994 *Phys. Rev.* B **44** 9667
[8] Feigelman M V, Geshkenbein V B, Larkin A I and Levit S 1993 *JETP Lett.* **57** 711; (1993 *Pis'ma Zh. Eksp. Teor. Fiz.* **57** 699)
[9] Harris J M, Yan Y F, Tsui O K C, Matsuda Y and Ong N P 1994 *Phys. Rev. Lett.* **73** 1711
[10] Bulaevskii L N, Larkin A I, Maley M P and Vinokur V M *Preprint*
[11] Nozieres P and Vinen W F 1966 *Phil. Mag.* **14** 667
[12] Ping Ao and Thouless D J 1992 *Phys. Rev. Lett.* **70** 2158
[13] Feigelman M V, Geshkenbein V B, Larkin A I and Vinokur V M *Preprint*
[14] Abrikosov A A 1988 *Fundamentals of the Theory of Metals* (Amsterdam: North-Holland) p 505
[15] Bardeen J and Stephen M J 1965 *Phys. Rev.* **140** A1197
[16] Dolgov O V and Khomskii D 1994 *Physica* C **235–240** 2951
[17] Gorkov L P and Kopnin N B 1975 *Usp. Fiz. Nauk* **116** 413; (1975 *Sov. Phys.–Usp.* **18** 496)
[18] Guinea F and Pogorelov Yu 1995 *Phys. Rev. Lett.* **74** 462
[19] Beasley M R, Labusch R and Webb W W 1969 *Phys. Rev.* **181** 682
[20] Campbell A M 1971 *J. Phys. C: Solid State Phys.* **2** 1492; 1971 *J. Phys. C: Solid State Phys.* **4** 3186
[21] Gittleman J I and Rosenblum B 1966 *Phys. Rev. Lett.* **16** 734
[22] Buzdin A and Feinberg D 1994 *Physica* C **235–240** 2755
[23] Hebard A F, Gammel P L, Rice C E and Levi A F J 1989 *Phys. Rev.* B **40** 5243
[24] Wu D H and Sridhar S 1990 *Phys. Rev. Lett.* **65** 2074
[25] Martinoli P, Fluckiger Ph, Marsico V, Srivastava P K, Leemann Ch and Gavilano J L 1990 *Physica* B **165 and 166** 1163
[26] Coffey M W and Clem J R 1991 *Phys. Rev. Lett.* **67** 386
[27] Brandt E H 1992 *Phys. Rev. Lett.* **67** 2219
[28] Wu Dong Ho, Booth J C and Anlage S M 1995 *Phys. Rev. Lett.* **75** 525
[29] Yeh N C 1991 *Phys. Rev.* B **43** 523
[30] Hsu T C 1992 *Phys. Rev.* B **46** 3680; 1993 *Physica* C **213** 305
[31] Choi E J, Lihn H T S, Drew H D and Hsu T C 1994 *Phys. Rev.* B **49** 13 271
[32] Miller D, Richards P L and Merchant P 1995 *Phys. Rev.* B **51** 8385
[33] Golosovsky M, Naveh Y and Davidov D 1992 *Phys. Rev.* B **45** 7495
[34] van der Beek C J, Geshkenbein V B and Vinokur V M 1993 *Phys. Rev.* B **48** 3393
[35] Nguyen P P, Oates D E, Dresselhaus G, Dresselhaus M S and Anderson A C 1995 *Phys. Rev.* B **51** 6686
[36] Golosovsky M A, Snortland H J and Beasley M R 1995 *Phys. Rev.* B **51** 6462
[37] Sridhar S 1994 *Appl. Phys. Lett.* **65** 1054
[38] Coffey M W 1992 *Phys. Rev.* B **46** 567
Sonin E B and Tagantsev A K 1991 *Supercond. Sci. Technol.* **4** 119
[39] Larkin A I and Ovchinnikov Yu N 1975 *Zh. Eksp. Teor. Fiz.* **68** 1915; (1976 *Sov. Phys.–JETP* **41** 960)
[40] Doettinger S G, Huebner R P, Gerdermann R, Kuhle A, Anders S, Trauble T G and Villegier J C 1994 *Phys. Rev. Lett.* **73** 1691
[41] Olsson H K, Koch R H, Eidelloth W and Robertazzi R P 1991 *Phys. Rev. Lett.* **66** 2661
[42] Wu H, Ong N P and Li Y Q 1993 *Phys. Rev. Lett.* **71** 2642
[43] Ando Y, Kubota H, Sato Y and Terasaki I 1994 *Phys. Rev.* B **50** 9680
[44] Yeh N C, Kriplani U, Jiang W, Reed D S, Strayer D M, Barner J B, Hunt B D, Foote M C, Vasquez R P, Gupta A and Kussmaul A 1993 *Phys. Rev.* **48** 9861
[45] Morgan D C, Zhang Kuan, Bonn D A, Liang Ruixing, Hardy W N, Kallin C and Berlinsky A J 1994 *Physica* C **235–240** 2015
[46] Huang M X, Bhagat S M, Findikoglu A T, Venkatesan T, Manheimer M A and Tyagi S 1992 *Physica* C **193** 421
[47] Zuo F, Salamon M B, Bukowski E D, Rice J P and Ginsberg D M 1990 *Phys. Rev.* B **41** 6600
[48] Blackstead H A, Pulling D B, McGinn P J and Clough C A 1991 *Physica* C **175** 534
[49] Golosovsky M, Ginodman V, Shaltiel D, Gerhouser W and Fischer P 1993 *Phys. Rev.* B **47** 9010
[50] Philipp A, Awasthi A M and Gruner G *Preprint*
[51] Owliaei J, Sridhar S and Talvacchio J 1992 *Phys. Rev. Lett.* **69** 3366
[52] Pambianchi M S, Wu D H, Ganapathi L and Anlage S M

1993 *IEEE Trans. Appl. Supercond.* **3** 2774
[53] Golosovsky M, Tsindlekht M, Chayet H and Davidov D 1994 *Phys. Rev.* B **50** 470; 1995 *Phys. Rev.* B **51** 12 062
[54] Ghosh I S, Cohen L F, Gallop J C, Caplin A D and Somekh R 1994 *Physica* C **235–240** 3157
[55] Revenaz S, Oates D E, Labbe-Lavigne D, Dresselhaus G and Dresselhaus M S 1994 *Phys. Rev.* B **50** 1178
[56] Xavier P, Buisson O and Richard J 1994 *Physica* C **235–240** 3229
[57] Anand N and Tinkham M 1995 *Phys. Rev.* B **52** 3789
[58] Booth J C, Wu D H and Anlage S M 1994 *Rev. Sci. Instrum.* **65** 2082
[59] Matsuda Y, Ong N P, Yan Y F, Harris J M and Peterson J B 1994 *Phys. Rev.* B **49** 4380
[60] Marcon R, Fastampa R, Giura M and Silva E 1991 *Phys. Rev.* B **43** 2940
[61] Maeda A, Iino Y, Hanaguri T, Motohira N, Kishio K and Fukase T 1995 *Phys. Rev. Lett.* **74** 1202
[62] Hanaguri T, Iino Y, Maeda A, Motohira N and Kishio K 1994 *Physica* C **235–240** 1991. (Note that the definition of the pinning constant adopted in this work differs from that used throughout our paper by the factor B/Φ_0.)
[63] Hein M, Piel H, Strupp M, Trunin M R and Portis A M 1992 *J. Magn. Magn. Mater.* **104–107** 529
[64] Golosovsky M, Davidov D, Farber E, Schieber M and Tsach T 1991 *Phys. Rev.* B **43** 10 390
[65] Parks B, Spielman S, Orenstein J, Nemeth D T, Ludwig F, Clark J, Merchant P and Lew D J 1995 *Phys. Rev. Lett.* **74** 3265
[66] Karrai K, Choi E J, Dunmore F, Liu S, Drew H P, Li Qi, Fenner D B, Zhu Y D and Zhang Fu-Chun 1992 *Phys. Rev. Lett.* **69** 152
[67] Kim Y B, Hempstead C F and Strnad A R 1962 *Phys. Rev. Lett.* **9** 306
[68] Kunchur M N, Christen D K and Phillips J M 1993 *Phys. Rev. Lett.* **70** 998
[69] Harris J M, Ong N P, Matl P, Gagnon R, Taillefer L, Kimura T and Kitazawa K 1995 *Phys. Rev.* B **51** 12 053
[70] Doyle R A, Campbell A M and Somekh R E 1993 *Phys. Rev. Lett.* **71** 4241
[71] Ziese M, Esquinazi P and Braun H F 1994 *Supercond. Sci. Technol.* **7** 869
[72] Farrell D E, Rice J P, Ginsberg D M and Liu J Z 1990 *Phys. Rev. Lett.* **64** 1573
Yethiraj M, Mook H A, Wignall G D, Cubitt R, Forgan E M, Lee S L, Paul D M and Armstrong T 1993 *Phys. Rev. Lett.* **71** 3019
[73] Shi X D, Chaikin P M, Ong N P and Wang Z Z 1994 *Phys. Rev.* B **50** 13 845
[74] Fiory A T 1971 *Phys. Rev. Lett.* **27** 501
[75] Sonin E B, Tagantsev A K and Traito K B 1992 *Phys. Rev.* B **46** 5830
[76] Caroli C and Maki K 1967 *Phys. Rev.* **159** 306
[77] Thompson R S 1970 *Phys. Rev.* B **1** 327
[78] Koetzler J, Nakielski G, Baumann M, Behr R, Goerke F and Brandt E H 1994 *Phys. Rev.* B **50** 3384
[79] Fisher D S, Fisher M P A and Huse D A 1991 *Phys. Rev.* B **43** 130
[80] Giura M, Marcon R, Silva E and Fastampa R 1992 *Phys. Rev.* B **46** 5753
[81] Sarti S, Fastampa R, Giura M, Silva E and Marcon R 1995 *Phys. Rev.* B **52** 3734
[82] Kim B F, Moorjani K, Adrian F J and Bohandy J 1991 *Appl. Phys. Lett.* **69** 4143
[83] Chen N J, Owliaei J and Sridhar S 1994 *Rev. Sci. Instrum.* **65** 2635
[84] Lederman D, Vier D C, Mendoza D, Santamaria J, Schultz S and Schuller I K 1995 *Appl. Phys. Lett.* **66** 3677
[85] Halbritter J 1990 *J. Appl. Phys.* **68** 6315
[86] Golosovsky M, Tsindlekht M, Chayet H, Davidov D, Bontemps N, Chocron S, Iskevitch E, Brodskii B and Contour J P 1994 *Physica* C **235–240** 3147
[87] Abulafia Y, Shaulov A, Wolfus Y, Prozorov R, Burlachkov L, Yeshurun Y, Majer D, Zeldov E and Vinokur V M 1995 *Phys. Rev. Lett.* **75** 2404
[88] Schalk R M, Samadi Hosseinali G, Weber H W, Proyer S, Schwab P, Bauerle D and Grunorfer S 1994 *Phys. Rev.* B **49** 3511
[89] Thrane B P, Dumas J, Schlenker C, Dubourdieu C, Senateur J P and Thomas O 1994 *Physica* C **235–240** 3047
[90] Monceau P, Saint-James D and Waysand G 1978 *Phys. Rev.* B **12** 3673
[91] Sonin E B and Traito K B 1994 *Phys. Rev.* B **50** 13 547
[92] Rosenblum B, Cardona M and Fischer G 1964 *RCA Rev.* **25** 491
[93] Doyle R A, Seow W S, Johnson J D, Walker D W, Campbell A M, Doyle T B, Somekh R E and Evetts J E *Proc. 7th. IWCC (Alpbach 1994)*
[94] Burlachkov L 1993 *Phys. Rev.* B **47** 8056
[95] Sarti S, Fastampa R, Giura M, Marcon R and Silva E 1994 *Physica* C **235–240** 3047
[96] Kogan V G and Clem J R 1981 *Phys. Rev.* B **24** 2497
[97] Blatter G, Geshkenbein V B and Larkin A I 1992 *Phys. Rev. Lett.* **68** 875
[98] Hao Z and Clem J R 1992 *Phys. Rev.* B **46** 5853; 1991 *Phys. Rev.* B **43** 7622
[99] Klemm R A 1993 *Phys. Rev.* B **47** 14 630
[100] Tachiki M and Takahashi S 1989 *Solid State Commun.* **70** 291
[101] Lofland S E, Bhagat S M, Rajeswari M, Venkatesan T, Kanjilal D, Senapati L and Mehta G K 1995 *Phys. Rev.* B **51** 8489
[102] Hylton T L and Beasley M R 1990 *Phys. Rev.* B **42** 11 669
[103] Deutscher G and Muller K A 1987 *Phys. Rev. Lett.* **59** 1745
[104] Salamon M B and Bardeen J 1987 *Phys. Rev. Lett.* **59** 2615
[105] Liang Ruixing, Dosanjh P, Bonn D A, Hardy W N and Berlinsky A J 1994 *Phys. Rev.* B **50** 4212
[106] Koshelev A E and Vinokur V M 1991 *Physica* C **173** 465
[107] Senoussi S, Oussena M, Collin G and Campbell I A 1988 *Phys. Rev.* B **37** 9792
[108] Larkin V A 1992 *Thesis* Chernogolovka, Institute of Solid State Physics
[109] Kes P H 1991 *Physica* C **185–189** 288
[110] Welp U, Kwok W K, Grabtree G W, Vandervoort K V and Liu J Z 1992 *Phys. Rev. Lett.* **69** 152
[111] de Nivelle M J M E, Gerritsma G J and Rogalla H 1994 *Physica* C **233** 185
[112] Bonn D A *et al* 1993 *Phys. Rev.* B **47** 11 314
[113] Schlesinger Z, Collins R T, Holtzberg F, Feild C, Blanton S H, Welp U, Grabtree G W, Fang Y and Liu J Z 1990 *Phys. Rev. Lett.* **65** 801
[114] Bulaevskii L N, Cho J H, Maley M P, Kes P, Li Qiang, Suenaga M and Ledvij M 1994 *Phys. Rev.* B **50** 3507